CHEMICAL ENGINEERING TRANSACTIONS
VOL. 66, 2018
A publication of AIDIC
The Italian Association of Chemical Engineering
Online at www.aidic.it/cet
Guest Editors: Songying Zhao, Yougang Sun, Ye Zhou
Copyright © 2018, AIDIC Servizi S.r.l.
ISBN 978-88-95608-63-1; **ISSN** 2283-9216
DOI: 10.3303/CET1866055

Analysis of Thermal Defects on Exterior Wall Insulation System

Yang Wang[a,*], Xiaoyu Hu[b], Shiyong Wu[a], Cheng Zhang[a]

[a]Department of Building Engineering, Hefei University, Hefei 230601, China
[b]School of Management, Jinan University, Guangzhou 510632, China
122432892@qq.com

This paper aims to evaluate the damage degree and actual effect of the exterior wall insulation system. For this purpose, the author decided to investigate a typical building with severe damages on the exterior wall insulation system. Then, the variation in temperature and humidity of the wall was measured by embedded sensors, and compared with the results obtained through theoretical analysis. Coupled with thermal image, the contrastive results help to clarify the causes and solutions to defects like exfoliation and leakage. This research provides new insights on the construction, application and repair of energy-saving walls.

1. Introduction

External thermal insulation has developed rapidly in China in recent years, However, there are still several problems concerning the application of this technology. For instance, an external thermal insulation system may not live to its designed service life (Abdelhafez et al., 2016), because its durability is affected by many adverse environmental factors. A system satisfying all energy-saving standards does not necessarily have a good practical effect.

Field tests are needed to verify whether the actual system can reach the designed life (Gschösser et al., 2012). Nevertheless, there is little report on the field test of the thermal insulation effect. What is worse, all external thermal insulation products are still in the trail-and-error phase. Many poor-quality products have entered the market, and the construction technology is still relatively backward. All these factors are restricting the actual effect of external thermal insulation (Feng et al., 2016).

It has been less than a decade since the application of external thermal insulation to walls in hot-summer/cold-winter zones in China. Despite the short history, various unfavourable factors have emerged, including but not limited to high humidity, excessive dryness and extreme weather (Delgado and Ramos, 2012). Large scale rectification and repair are wanted for the exterior wall insulation system.

This research targets a typical building with severe damages on the exterior wall insulation system. Completed at the end of 2012, the building has been in service for only 6 years. However, hollow defects and partial exfoliation are commonplace on its external façade, which pose a great threat to safety. The damage degree and actual effect of the exterior wall insulation system must be evaluated before any partial or overall repair (Manoosingh, 2016).

2 Methodology

2.1 Experiment design

NiCr-Ni thermocouple sensors were pasted in several areas between the structure layer and thermal insulation layer of the wall. Then, the sensors were connected to a desktop data acquisition device (Alborn MU-56901), which supports automatic acquisition of data and real-time recording of interior temperature (Figure 1). Moreover, a handheld data collector (Alborn 2908) was adopted to measure the water content of the wall surface. In the connector, the FHA696 sensors can capture the internal moisture content (Li et al., 2013), and the FHA6X6 sensors can determine the relative humidity of the internal air layer. The surface temperature of the wall is measured by an infrared thermometer (Lohonyai et al., 2015).

Please cite this article as: Wang Y., Hu X., Wu S., Zhang C., 2018, Analysis of thermal defects on exterior wall insulation system, Chemical Engineering Transactions, 66, 325-330 DOI:10.3303/CET1866055

Figure 1: data acquisition device and testing site

In addition, a B360 infrared thermograph (FLIR Systems) was employed to detect the exfoliation and leakage on the external wall (Barreira and Freitas, 2007). The two phenomena and their detection methods are briefly introduced below.

The exfoliation occurs when the face layer and insulation layer break off from the structure layer under the action of changing humidity and temperature. Once exfoliation happens, a layer of air will appear in the wall structure. With a low heat capacity, the air layer reduces the thermal conductivity of the wall, and suppresses the heat conduction between the exfoliated area and the main wall (Yu et al., 2011). Any change in external temperature will lead to obvious difference in temperature distribution across the wall, forming hot spots and cold spots. This difference can be captured by the infrared thermograph (Cristea and Burges, 2009).

The leakage refers to the infiltration of rainwater through the microcracks on the waterproof layer and the insulation layer. Because of the high heat capacity of water, there will be a huge difference between leaked area and normal area in surface temperature distribution with the changes in external temperature. This difference can also be detected easily by the infrared thermograph.

2.2 Experimental procedure

2.2.1 Wall structure

The object is a homogenous flat wall consisting of four layers mainly. Field test reveals that the actual thickness was very different from the designed value. The designed and actual thicknesses are recorded in Table 1.

Table 1: Wall structure of main body

Wall material (From outside to inside)	*Designed thickness (mm)*	*Actual thickness (mm)*	*Thermal conductivity W/(m^2 • K)*
Anti-crack mortar	8	5	0.930
Glazed hollow bead Insulation mortar	40	28	0.0803
Coal gangue sintered hollow brick	200	200	0.580
Lime mortar	20	12	0.810

For the materials in Table 1, the anti-crack mortar was added with anti-cracking agents like acrylic resin; the glazed hollow bead insulation mortar, the key to thermal insulation, is a silica lava material mainly contains SiO_2, supplemented by ingredients like fly ash, ordinary Portland cement, polypropylene fibre and special compound rubber powder. Among them, the cement, consisting of SiO_2, Al_2O_3 and CaO, might corrode other materials due to its alkalinity. Coal gangue sintered hollow brick is mainly composed of SiO_2 and the lime mortar mainly composed of $Ca(OH)_2$.

Several thermal experiments were conducted in winter, during which the indoor air temperature was maintained constant for over 2 hours. The multilayer flat wall was simulated by a 1D steady-state heat transfer model. The thermal conductivity data came from the drawings on energy-saving design. Without considering the air layer of coal gangue sintered hollow brick, the heat transfer calculation only computed the overall thermal resistance (Olhager and Johansson, 2012).

Six sensors were embedded on each façade between the structure layer and the insulation layer. Together, these sensors acquired the temperature automatically at regular intervals. The indoor and outdoor

environment temperatures were measured by a thermo-hygrometer (Avci et al.,2013). The mean temperature was obtained by minimum mean-variance method (Hamed and Wahid, 2012).

2.2.2 Numerical example

This subsection compares the theoretical temperature of the designed wall thickness and the measured temperature of the actual wall thickness. According to field measurement, the indoor and outdoor environment temperatures were respectively 20.84℃ and -10.46℃. Referring to thermal parameters, the heat transfer resistances of the inner and outer surfaces were respectively R_i=0.11 ($m^2 \cdot K/W$) and R_e=0.04 ($m^2 \cdot K/W$). The heat transfer resistance of wall was calculated as $R_0=R_i+\sum R+R_e$=1.03 $m^2 \cdot K/W$ and the heat flux of wall as $q=(t_i-t_e)/R_0$=30.51 $W/m^2 \cdot K$.

The internal temperature distribution was as follows:

$\theta_i= t_i -(t_i-t_e)\ R_i\ /R_0$=17.48℃

$\theta_2= t_i -(ti-t_e)\ (R_i + R_1)/R_0$=16.72℃

$\theta_3= t_i -(t_i-t_e)\ (R_i + R_1 + R_2)/R_0$=6.20℃

$\theta_4= t_i -(t_i-t_e)\ (R_i + R_1 + R_2+ R_3)/R_0$=-8.97℃

$\theta_e= t_i -(t_i-t_e)\ (R_0 - R_e)/R_0$=-9.24℃

The above calculation shows that the designed temperature on the interface between thermal insulation layer and structure layer was 6.20℃, much higher than the measured temperature of 1.84℃, which was much lower than design temperature. Considering that the actual thickness was smaller than the designed value, the interface temperature was calculated as 3.81℃ according to the actual thickness, which is still higher than the measured value.

2.2.3 Detection of exfoliation and leakage

The exterior wall was coated with tiles and waterproof materials. Most influencing factors were excluded, such as surface emissivity, angle of view, sight distance, temperature gradient, sunlight intensity, temperature, humidity, wind speed and heat radiation (Balaras and Argiriou, 2002). To locate the defects of exfoliation and leakage, thermal images were imported to the software Reporter 8.0 to distinguish normal morphologies from abnormal ones (Zhang et al., 2018).

The search for leakages was carried out on a sunny day after three days of raining. As shown in the rectangular purple area of Figure 2, a lot of leakage areas were discovered on the exterior wall. The leakage is a main reason for hollowing, surface cracking and exfoliation (Vemuri and Atadero, 2017).

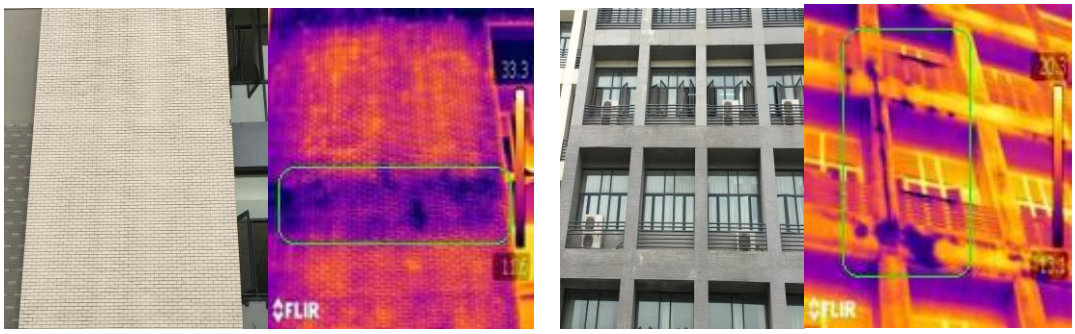

Figure 2: Thermal and visible images

3 Results and Analysis

3.1 Analysis of test results

The interface temperature between coal gangue-sintered brick layer and mortar layer were measured at five different times. Then, the theoretical temperatures were computed at the designed thickness and compared with the temperatures measured at actual thickness. In all cases, the measured temperatures were lower than the calculated temperatures.

Next, the partial pressure of water vapor (Ps) and that of saturated water vapour (P) of each layer were computed to determine the presence of leakage. Since there was no intersection between the two distribution lines of P and Ps (Figure 3), no condensation occurred in the wall, i.e. the water seepage in the wall must be caused by external factors.

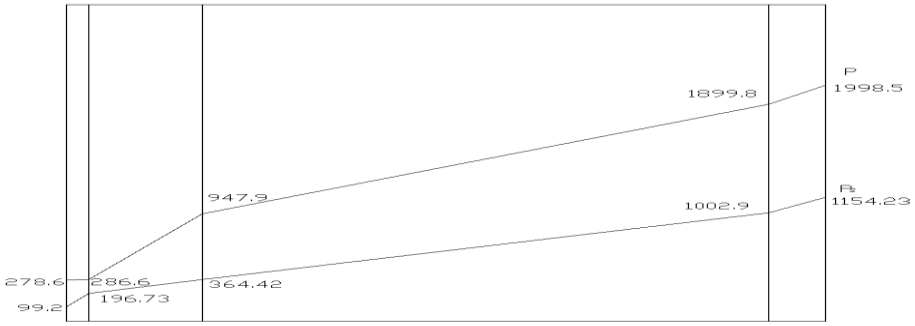

Figure 3: Distribution lines of P and Ps for wall structure of main body

In the air layer of coal gangue sintered hollow brick, the relative humidity measured by FHA6X6 sensors was above 90% for a long time. The exterior wall surface and mortar layer also had varied degrees of water contents after raining, as measured by FHA696 and FHA636 sensors.

Through the above analysis, it is learned that many auxiliary materials had serious defects, such as the protective layer, alkali-resistant glass fibre mesh, flexible putty (hydroxypropyl cellulose, $C_{36}H_{70}O_{19}$), anti-crack mortar (acrylic ester, CH_2=CHCOOR), waterproof mortar and elastic coating (acrylic resin ($C_3H_4O_2$)n). This goes against the requirements of the Technical Specification for External Thermal Insulation on Walls (JGJ144-2008).

The defects of the auxiliary materials induced the seepage of the wall and moistening of the insulation layer, leading to an obvious decline of insulation ability (Seo et al.,2013). Furthermore, the thermal insulation effect was weakened by the fact that the actual thickness of the insulation layer was below that the designed thickness. This calls for high-quality construction teams, strict implementation of standards and rigorous construction management.

3.2 Display effect of exfoliation on thermal images taken at different times

Taking the west façade of the target building for example, the thermal images on exfoliation obtained in the heating and cooling phases were imported to Reporter 8.0(Figure 4). Six temperature points were selected from the exfoliated area (group 1) and six from the normal area (group 2). According to the table generated by the software, the mean values were calculated for each group of data, and the difference between the two means (△t) was also obtained to judge the display effect of exfoliation（Cunningham *et al*.,2016）. A total of 18 thermal images were taken at different times, and all computations were carried out at the same place. The temperature difference curves were drawn and recorded in Figure 5.

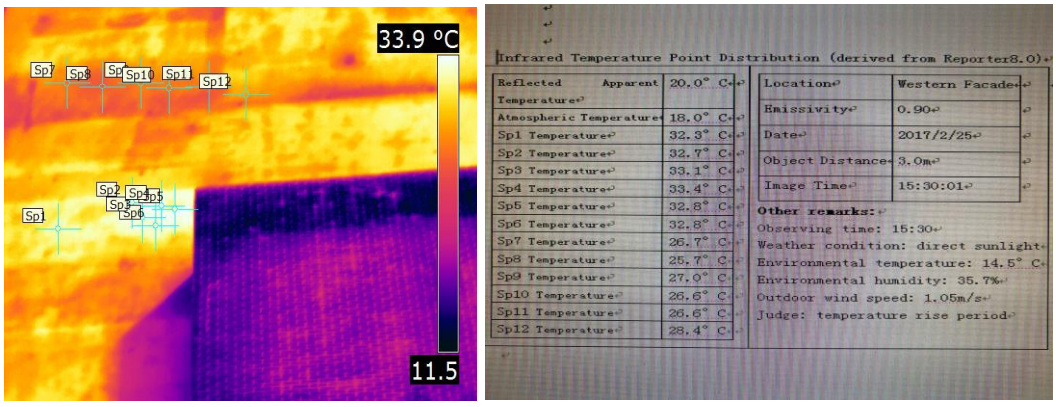

Figure 4: Thermal image and temperature points

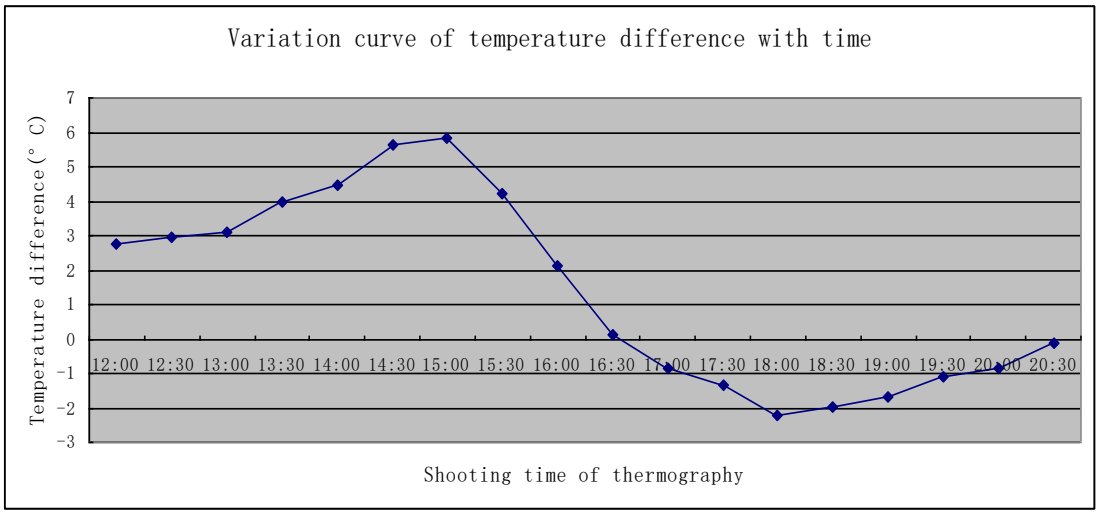

Figure 5: Temperature difference curves

As shown in Figure 5, there was a huge temperature difference in the heating phase. The mean difference of the 9 groups was 3.90℃ and the peak temperature reached 5.85℃. The best observation time fell between 14:00 and 15:30. A possible explanation is that the sunshine is stronger in this period during the winter. By contrast, the temperature difference was rather small in the cooling phase. The mean difference of the 9 groups was -1.11℃ and the peak temperature was -2.24℃. The best observation time fell between 17:30 and 19:00. This is probably because the temperature varies little when it is getting dark.

For intuitiveness, relatively high and low temperature areas were selected from the thermal image in the experiment. In actual practice, exfoliation defects could be identified well when the temperature difference between normal point and defect point reached 0.5℃. In the cooling phase, the thermal image boasts the optimal effect if the sunshine lasts for a while before it suddenly disappears.

4. Conclusions

In the target wall, the thermal insulation effect was reduced by the insufficient thickness of insulation layer, and worsened by the moisture absorption. There was no condensation in the wall and the water seepage in the wall must be caused by external factors. The poor thermal insulation effect of the building is mainly attributable to the substandard quality and quantity and the immature construction technology.

The thermal image offers a good way to identify exfoliation and leakage. The best observation time can also be determined accurately. According to the analysis results, the wall should be repaired in summer when it is easy to make contrast measurement. Thanks to the large temperature difference, the display effect of the thermal image must be better than that in winter.

Acknowledgments

This study received financial support from:

1. The Education Department of Anhui Province, China, 2018(Project Title: “Defect Analysis and Durability Study of Typical Exterior Wall Insulation Systems”, KJ2018A0559).
2. The Education Department of Anhui Province, China, 2016(Project Title: “The Study on the Sun-shading Strategy of Building Envelope in Anhui Area”, KJ2016A607).

Reference

Abdelhafez E.A., Hamdan M.A., Mohammad L.B., 2016, Effect of an Insulation Layer to Prevent Water Vapor Condensation along the Inside Surface of a Building Wall Using an Artificial Neural Network, Journal of Infrastructure Systems, 22(4), DOI: 10.1061/(ASCE)IS.1943-555X.0000207
and Building materials, 21, 218-224, DOI: 10.1016/j.conbuildmat.2005.06.049

Avci M., Erkoc M., Rahmani A., 2013, Model predictive HVAC load control in buildings using real-time electricity pricing, Energy and Buildings, 60 ,199–209, DOI: 10.1016/j.enbuild.2013.01.008

Balaras C.A., Argiriou A.A., 2002, Infrared thermography for building diagnostics, Energy and Buildings, 34, 171-183, DOI: 10.1016/S0378-7788(01)00105-0

Barreira E., Freitas V.P., 2007, Evaluation of building materials using infrared thermography, Construction
Cristea N.C., Burges S.J., 2009, Use of Thermal Infrared Imagery to Complement Monitoring and Modeling of Spatial Stream Temperatures, J. Hydrol. Eng., 14, 1080-1090, DOI: 10.1061/ASCEHE.1943-5584.0000072
Cunningham C., Whittaker W., Nesnas L., 2016, Detecting Loose Regolith in Lunar Craters Using Thermal Imaging, 15th Biennial ASCE Conference on Engineering, Science, Construction, and Operations in Challenging Environments, April 11–15, 2016|Orlando, Florida, DOI: 10.1061/9780784479971.003
Delgado J.M.P.Q., Ramos N.M.M., 2012, Application of different transient sorption methods to evaluate moisture diffusion coefficients of building materials on the hygroscopic range, Journal of Building Physics, 35, 251-266, DOI: 10.1177/1744259111418331
Feng R., Li J., Li X.Z., 2016, Performance Study of External Wall Insulation and a Hybrid Energy Supply System for a Rural Residential Building, Journal of Energy Engineering, 142, 05016003, DOI: 10.1061/(ASCE)EY.1943-7897.0000366
Gschösser F.L., Wallbaum H., Boesch M.E., 2012, Life-Cycle Assessment of the Production of Swiss Road Materials, Journal of Materials In Civil Engineering, 168-176, DOI: 10.1061/(ASCE)MT.1943-5533.0000375
Hamed H.S., Wahid M., 2012, Numerical modelling and experimental investigations of thermal performance of reflective insulations, Journal of Building Physics, 36, 163-177, DOI: 10.1177/1744259112444021
Hauser G., Kersken M., Sinnesbichler H., 2013, Experimental and numerical investigations for comparing the thermal performance of infrared reflecting insulation and of mineral wool, Energy and Buildings, 58,131–140, DOI: 10.1016/j.enbuild.2012.10.033
Li H., Harvey J., Kendall A., 2013, Field measurement of albedo for different land cover materials and effects on thermal performance, Building and Environment, 59, 536-546, DOI: 10.1016/j.buildenv.2012.10.014
Lohonyai A.J., Korany Y., Gül M., 2015, Remote Field Monitoring of Thermal and Moisture Deformations in Masonry Cavity Wall Building Envelopes, Journal of Performance of Constructed Facilities, 29. DOI: 10.1061/(ASCE)CF.1943-5509.0000550
Manoosingh C., 2016, Improving the Thermal Efficiency and Environmental Sustainability of Building Insulation, Construction Research Congress 2016, 1163-1170, DOI: 10.1061/9780784479827.117
Olhager J., Johansson P., 2012, Linking long-term capacity management for manufacturing and service operations, J. Eng. Technol. Manage., 29, 22–33, DOI: 10.1016/j.jengtecman.2011.09.003
Seo S., Wang C.H., Grozev G., 2013, Cooling energy consumption and reduction effect for residential buildings in South East Queensland, Australia, Building and Environment, 59, 408-416, DOI: 10.1016/j.buildenv.2012.09.006
Vemuri S.H., Atadero R.A., 2017, Case Study on Rapid Scanning Techniques for Concrete Bridge Decks with Asphalt Overlay: Ground-Penetrating Radar and Infrared Thermography, Pract. Period. Struct. Des. Constr., 22, 05016004, DOI: 10.1061/(ASCE)SC.1943-5576.0000313
Yu S., Bomberg M., Zhang X., 2011, Integrated methodology for evaluation of energy performance of the building enclosures, Journal of Building Physics, 35, 194-212, DOI: 10.1177/1744259111420071
Zhang X. M., Du Y. C., Li F., Ye X.Y., Liu Y., 2018, Expressway Visual Distance Detection Using Thermal Imager: Comparing Normal and Infrared Images, J. Transp. Eng., Part A: Systems, 144, 04018019, DOI: 10.1061/JTEPBS.0000144